

Local Gravitational Instability of Magnetized Shear Flows

Gregory G. Howes, Steven C. Cowley

*Department of Physics and Astronomy, University of California, Los Angeles, CA
90095-1547*

ghowes@physics.ucla.edu

and

James C. McWilliams

Department of Atmospheric Sciences, University of California, Los Angeles, CA 90095

ABSTRACT

The effect of magnetic shear and shear flow on local gravitationally induced instabilities is investigated. A simple model is constructed allowing for an arbitrary entropy gradient and a shear plasma flow in the Boussinesq approximation. A transformation to shearing magnetic coordinates achieves a model with plasma flow along the magnetic field lines where the coordinate lines are coincident with the field lines. The solution for the normal modes of the system depends on two parameters: the Alfvén Mach number of the plasma flow and the entropy gradient. The behavior of the unstable normal modes of this system is summarized by a stability diagram. Important characteristics of this stability diagram are the following: magnetic shear is stabilizing and the entropy gradient must exceed a threshold value for unstable mode growth to occur; flow acts to suppress mode growth in a substantially unstable regime as expected, yet near marginal stability it can lessen the stabilizing effect of magnetic shear and enhance the growth rates of the instability; and, as the Alfvén Mach number approaches one, the instability is completely stabilized. Analytical work is presented supporting the characteristics of the stability diagram and illuminating the physical mechanisms controlling the behavior of the model. A derivation of the stability criterion for the case without shear flow, asymptotic solutions in the limit that the Alfvén Mach number approaches one and in the limit of zero growth rate, a complete WKB solution for large growth rates, an exactly soluble bounded straight field case, and energy conservation relations are all presented. The implications of this work for astrophysical and fusion applications and the potential for future research extending the results to include compressibility are discussed.

Subject headings: MHD—gravitational instability—magnetic shear—velocity shear

1. Introduction

The gravitational stability of a fluid against convective motion has been extensively studied over the past century. Pioneering examinations of the stability of unmagnetized and magnetized compressible fluids have been conducted by Schwarzschild (1906), Newcomb (1961), and Parker (1979). These papers have had a profound influence on diverse subjects from the dynamics of astrophysical objects to the confinement of plasma in a fusion device. Here we examine the effects of shear in the magnetic field and of an applied shear plasma flow on stability against gravitational interchange. These effects change the stability properties and our results are important for many applications.

We construct a simple model to study the effects of magnetic shear and shear flow on the stability properties of a magnetized plasma in a gravitational field. We derive the equations which determine the behavior of this model in the Boussinesq limit. The equations depend on two parameters, the plasma flow Alfvén Mach number and the entropy gradient. We conduct a numerical study of the normal modes of instability and summarize the behavior of the unstable modes by a stability diagram. The stability diagram demonstrates three important characteristics. First, the entropy gradient must exceed a threshold value for unstable mode growth to occur. Therefore, the shear magnetic field can stabilize a nonzero entropy gradient. Second, as expected, shear flow does act to suppress unstable mode growth when the system is at a substantially unstable point in parameter space. But, surprisingly, near marginal stability, shear flow actually enhances the growth rates of the instability and also lowers the threshold entropy gradient necessary for instability. The effect of magnetic shear—to stabilize the plasma and increase the threshold entropy gradient—is diminished by the addition of shear flow. The system can extract energy from the shear flow to further drive the system to instability. Third, as the Alfvén Mach number approaches one, the unstable growth rate is suppressed; the normal modes of the instability are completely stabilized when the plasma flow exceeds the Alfvén speed. Here, the unstable region in space where a mode can grow moves faster than any perturbation in the system; any disturbance will be swept downstream out of the unstable region, leaving behind a stable plasma.

Analytical work helps us to understand the mechanisms responsible for these characteristics. First, the stability criterion for the case without shear flow is derived demonstrating that a shear magnetic field can support a positive entropy gradient. Next, asymptotic solutions demonstrate analytically that stabilization occurs as the Alfvén Mach number approaches one, yet the threshold entropy gradient for instability goes to zero in the same limit. In addition, a complete WKB solution in the limit of a large growth rate demonstrates both the stabilization by flow at large growth rates and destabilization near marginal stability. Then, a bounded straight field case is solved exactly to show that the lowering of the thresh-

old entropy gradient with increased shear flow is a characteristic of plasma flow along the field lines and not dependent on the magnetic shear in the general model. Finally, energy conservation relations are derived and analyzed.

In section 2, we describe the model under consideration and derive the governing system of equations. The numerical stability analysis for the general model and the stability diagram are presented in section 3.1. Section 3.2 contains the analytical results illuminating the characteristics of the stability diagram. We describe an exactly soluble, bounded, straight-field case in section 3.3. Finally, in section 4, the implications of this work on galactic physics, accretion disk physics, solar physics, and tokamak confinement are discussed.

2. Derivation of Equations

In this section, we derive the equations for linear perturbations of a vertically stratified atmosphere with shear magnetic field and shear flow in the high- β , or Boussinesq, limit. We motivate and apply a coordinate transformation which casts the problem in its most natural form. Investigating the limit of the most unstable modes, we derive a system of three coupled first-order ordinary differential equations which capture the lowest order behavior of the model.

2.1. Setup and Coordinate Transformation

Consider a stationary state for an ideal plasma with mass density $\rho(x)$ and thermal pressure $p(x)$ and an embedded horizontal shear magnetic field given by

$$\mathbf{B}_0 = B_0 \left(\hat{\mathbf{z}} + \frac{x}{l_B} \hat{\mathbf{y}} \right). \quad (1)$$

We then impose a shear flow on this plasma given by

$$\mathbf{v}_0 = v_0 \frac{x}{l_v} \hat{\mathbf{y}}, \quad (2)$$

and include gravitational acceleration in the vertical direction given by $\mathbf{g} = -g\hat{\mathbf{x}}$. Equilibrium force balance yields

$$\frac{\partial}{\partial x} \left(p + \frac{B^2}{8\pi} \right) = -g\rho. \quad (3)$$

Figure 1 shows the geometry of this shear magnetic field as well as the imposed shear flow on the system.

The instabilities of this plasma are expected to have a short perpendicular wavelength and a long parallel wavelength (with respect to the magnetic field) so as to maximize motion in the vertical direction and minimize field line bending (Newcomb 1961). Short perpendicular wavelengths, however, are rapidly sheared apart by the perpendicular shear flow. We would thus like to transform to a coordinate system with two properties: first, that the flow is along the magnetic field lines; and, second, that field lines are coordinate lines. The application of sheared coordinate systems to simplify a problem of this nature is well documented. Roberts and Taylor (1965) employed a coordinate system in which the field lines are coincident with the coordinate lines to describe the Rayleigh-Taylor instability of a fluid supported by a shear magnetic field; Goldreich and Lynden-Bell (1965) used a shearing coordinate system to attack the problem of local gravitational instabilities in a system with shear flow arising from differential rotation.

We transform the shear velocity to a parallel velocity by transforming to a frame moving in z

$$z' = z + v_f t. \quad (4)$$

where $v_f = \frac{l_B}{l_v} v_0$. In this transformed frame, the velocity becomes

$$\mathbf{v}' = \mathbf{v}_f + \mathbf{v}_0 = v_f \left(\hat{\mathbf{z}} + \frac{x}{l_B} \hat{\mathbf{y}} \right),$$

i.e. parallel to \mathbf{B}_0 . We construct field line coordinates by transforming the y coordinate to

$$y' = y - \frac{xz'}{l_B}. \quad (5)$$

The x coordinate is left unchanged, $x' = x$. It is easy to verify that x' and y' are constant along field lines ($\mathbf{B}_0 \cdot \nabla x' = \mathbf{B}_0 \cdot \nabla y' = 0$) and that $\mathbf{B} = B_0 \nabla x' \times \nabla y'$. The surfaces of constant y' twist from vertical at $z' = 0$ to almost horizontal as $z' \rightarrow \pm\infty$. This geometry is shown in Figure 1.

At first, introducing the field line coordinates seems unhelpful since it introduces explicit z' dependence into the equations. The problem also has x dependence that arises from the variation of \mathbf{B} , $p(x)$, and $\rho(x)$. Indeed, one way to tackle this problem is to Fourier transform in y and z and solve for the x dependence. However, the lowest order solution in the twisting coordinate system is a superposition of these Fourier modes, or, complementarily, a Fourier solution can be constructed by a superposition of these twisting modes (Roberts and Taylor 1965). We summarize the relationship between these representations in Appendix A. We consider the solutions in the twisting coordinates to be more physically relevant since they are localized in z' .

2.2. Application of Ideal MHD

The basic equations of ideal MHD include the momentum equation written in terms of the gradient of total pressure (thermal and magnetic), the magnetic tension force, and the gravitational force,

$$\rho \frac{D\mathbf{v}}{Dt} = -\nabla \left(p + \frac{\mathbf{B}^2}{8\pi} \right) + \frac{\mathbf{B} \cdot \nabla \mathbf{B}}{4\pi} + \rho \mathbf{g}, \quad (6)$$

the induction equation in the limit of zero resistivity,

$$\frac{\partial \mathbf{B}}{\partial t} = \nabla \times (\mathbf{v} \times \mathbf{B}), \quad (7)$$

the continuity equation,

$$\frac{D\rho}{Dt} = -\rho \nabla \cdot \mathbf{v}, \quad (8)$$

and the adiabatic equation of state,

$$\frac{D}{Dt} \left(\frac{p}{\rho^\Gamma} \right) = 0. \quad (9)$$

Here $\frac{D}{Dt} = \frac{\partial}{\partial t} + \mathbf{v} \cdot \nabla$ denotes the Lagrangian derivative, \mathbf{v} represents the plasma velocity, and Γ is the adiabatic index. These equations must be evolved subject to the constraint that

$$\nabla \cdot \mathbf{B} = 0. \quad (10)$$

Equations (6)-(9), linearized about the equilibrium (equations (1)-(3)), yield:

$$\left(\gamma' + v_f \frac{\partial}{\partial z'} \right) \delta \mathbf{v} + \delta \mathbf{v} \cdot \nabla \mathbf{v}_0 = -\frac{1}{\rho_0} \nabla \left(\delta p + \frac{B_0 \delta B_{\parallel}}{4\pi} \right) + \frac{B_0}{4\pi \rho_0} \frac{\partial \delta \mathbf{B}}{\partial z'} + \frac{\delta \mathbf{B} \cdot \nabla \mathbf{B}_0}{4\pi \rho_0} - \frac{g \delta \rho \hat{\mathbf{x}}}{\rho_0} \quad (11)$$

$$\left(\gamma' + v_f \frac{\partial}{\partial z'} \right) \delta \mathbf{B} + \delta \mathbf{v} \cdot \nabla \mathbf{B}_0 = B_0 \frac{\partial \delta \mathbf{v}}{\partial z'} + \delta \mathbf{B} \cdot \nabla \mathbf{v}_0 - \mathbf{B}_0 \nabla \cdot \delta \mathbf{v} \quad (12)$$

$$\left(\gamma' + v_f \frac{\partial}{\partial z'} \right) \delta \rho = -\delta \mathbf{v} \cdot \nabla \rho_0 - \rho_0 \nabla \cdot \delta \mathbf{v} \quad (13)$$

$$\left(\gamma' + v_f \frac{\partial}{\partial z'} \right) \delta p = -\delta \mathbf{v} \cdot \nabla p_0 - \Gamma p_0 \nabla \cdot \delta \mathbf{v}, \quad (14)$$

where we have taken all quantities to vary in time as $e^{\gamma' t}$.

In a straight field (Newcomb 1961) and a shear field (Roberts and Taylor 1965) without flow, the most unstable perturbations are incompressible to lowest order and have a small horizontal perpendicular wavelength. Such perturbations maximize vertical motion which

extracts energy from the gravitational potential energy and minimize horizontal motions which extract no energy. To isolate these motions, we impose the ordering

$$\frac{\partial}{\partial y'} = ik \sim \mathcal{O}\left(\frac{\epsilon^{-1}}{l_B}\right) \quad (15a)$$

$$\frac{\partial}{\partial x'} \sim \mathcal{O}\left(\frac{\epsilon^{-1/2}}{l_B}\right) \quad (15b)$$

$$\frac{\partial}{\partial z'} \sim \mathcal{O}\left(\frac{1}{l_B}\right) \quad (15c)$$

$$\frac{x'}{l_B} \sim \mathcal{O}(\epsilon^{1/2}). \quad (15d)$$

where $\epsilon = (kl_B)^{-1} \ll 1$ is the ordering parameter of our problem. Clearly, all perturbed quantities vary as $e^{iky'}$. It is also convenient to define the vectors,

$$\mathbf{b} = \frac{\mathbf{B}_0}{B_0} \quad (16a)$$

$$\mathbf{e}_\wedge = \nabla y' \quad (16b)$$

$$\mathbf{e}_\perp = \frac{\nabla y' \times \mathbf{B}_0}{B_0}. \quad (16c)$$

The perturbed plasma velocity and magnetic field are projected along these directions, *i.e.*

$$\delta \mathbf{v} = \delta v_\perp \mathbf{e}_\perp + \delta v_\wedge \mathbf{e}_\wedge + \delta v_\parallel \mathbf{b}$$

$$\delta \mathbf{B} = \delta B_\perp \mathbf{e}_\perp + \delta B_\wedge \mathbf{e}_\wedge + \delta B_\parallel \mathbf{b}.$$

Note that the basis vectors \mathbf{e}_\perp , \mathbf{e}_\wedge , and \mathbf{b} are neither unit vectors nor constant in space—*e.g.*, $\mathbf{B}_0 \cdot \nabla \mathbf{e}_\wedge = -\frac{B_0}{l_B} \hat{\mathbf{x}}$. We expand all perturbed quantities in powers of $\epsilon^{1/2}$ and denote order as a superscript—for example, $\delta v_\perp = \sum_{n=0}^{\infty} \delta v_\perp^{(n)} \epsilon^{n/2}$. The ordered, perturbed quantities and operators are substituted into equations (11)–(14). Equations (12)–(14) at $\mathcal{O}(\epsilon^{-1})$ and the \mathbf{e}_\wedge projection of equation (12) yield

$$\delta v_\wedge^{(0)} = \delta B_\wedge^{(0)} = 0. \quad (17)$$

Thus, the dominant motion is along the constant y' surfaces in the \mathbf{e}_\perp direction. Equations (12)–(14) at $\mathcal{O}(\epsilon^{-1/2})$ produce

$$\nabla \cdot \left(\delta v_\perp^{(0)} \mathbf{e}_\perp + \delta v_\wedge^{(1)} \mathbf{e}_\wedge \right) = 0. \quad (18)$$

Thus, the perpendicular motion is incompressible to lowest order. At $\mathcal{O}(\epsilon^{-1})$, the \mathbf{e}_\wedge component of equation (11) gives

$$\delta p^{(0)} + \frac{B_0 \delta B_\parallel^{(0)}}{4\pi} = 0. \quad (19)$$

Equation (19) expresses the fact that, on the time scales of interest, pressure balance is achieved across the convective eddies (in the \mathbf{e}_λ direction). In a subsidiary expansion, we take the high- β , or Boussinesq, limit ($\beta = \frac{4\pi\rho_0}{B^2}$). Thus, equation (19) reduces to $\delta p^{(0)} = 0$, and we find from equation (14) that

$$\delta\mathbf{v}^{(0)} \cdot \nabla p_0 = -\Gamma p_0 (\nabla \cdot \delta\mathbf{v})^{(0)}. \quad (20)$$

At $\mathcal{O}(\epsilon^{-1/2})$, the \mathbf{e}_λ component of equation (11) yields $\delta p^{(1)} + \frac{B_0 \delta B_\parallel^{(0)}}{4\pi} = 0$, or taking the high- β limit, $\delta p^{(1)} = 0$. The final stability equations are obtained from the sum and difference of the \mathbf{e}_\perp projections of equations (11) and (12) at $\mathcal{O}(1)$ and from equation (13) using equation (20) to substitute for $\nabla \cdot \delta\mathbf{v}$. After some tedious but straightforward algebra, we obtain

$$-(1-M)\frac{dA_+}{dz} = -\gamma A_+ + (1+M)\frac{z}{1+z^2}A_- - \frac{s}{(1+z^2)^{1/2}} \quad (21)$$

$$(1+M)\frac{dA_-}{dz} = -\gamma A_- - (1-M)\frac{z}{1+z^2}A_+ + \frac{s}{(1+z^2)^{1/2}} \quad (22)$$

$$M\frac{ds}{dz} = -\gamma s - \frac{1}{2}\frac{A_+ - A_-}{(1+z^2)^{1/2}}s'_0, \quad (23)$$

where A_+ and A_- are the Elsässer variables defined by

$$A_+ = \frac{1}{(1+z^2)^{1/2}} \left(\frac{\delta B_\perp}{B_0} + \frac{\delta v_\perp}{v_A} \right) \quad (24)$$

$$A_- = \frac{1}{(1+z^2)^{1/2}} \left(\frac{\delta B_\perp}{B_0} - \frac{\delta v_\perp}{v_A} \right) \quad (25)$$

and the entropy is given by

$$s = \frac{gl_B}{v_A^2} \left(\frac{\delta\rho}{\rho_0} \right). \quad (26)$$

We have normalized so that $z = z'/l_B$ and $\gamma = \gamma'l_B/v_A$. Equations (21)–(23) contain two parameters: the Mach number of the plasma flow with respect to the Alfvén speed ($v_A = \frac{B_0}{(4\pi\rho)^{1/2}}$),

$$M = \frac{v_f}{v_A}, \quad (27)$$

and the entropy gradient,

$$s'_0 = \frac{gl_B^2}{v_A^2} \left(\frac{\rho'_0}{\rho_0} - \frac{p'_0}{\Gamma p_0} \right), \quad (28)$$

where the primes denote differentiation by x . With the boundary conditions that $A_+ \rightarrow 0$, $A_- \rightarrow 0$, and $s \rightarrow 0$ as $|z| \rightarrow \pm\infty$, equations (21)–(23) define an eigenvalue problem for γ . Solution of the stability equations yields $\gamma(M, s'_0)$.

Equations (21)–(23) have a simple physical interpretation. A_+ , the Alfvén wave going in the negative z (upstream) direction, travels at the (normalized) speed $1 - M$. The A_+ wave is coupled to the A_- wave by magnetic and velocity shear (the A_- term in equation [21]). The A_+ wave is driven by gravity via the s term in equation (21). A_- , the Alfvén wave going in the positive z (downstream) direction, travels at speed $1 + M$, is coupled to A_+ , and is driven by s . The variable s is proportional to the density or entropy perturbation and it is driven by both Alfvén waves, as seen in equation (23).

3. Stability Analysis

In this section, we discuss the unstable eigenvalues ($\mathbf{Re} \gamma > 0$) and eigenfunctions of equations (21)–(23). We have not examined the stable part of the spectrum in detail although numerical results indicate a continuum along the imaginary γ axis. Two properties of equations (21)–(23) show that it is sufficient to examine stability in the region $0 \leq M \leq 1$. First, note that $\gamma(-M, s'_0) = \gamma(M, s'_0)$ since we can map equations (21)–(23) onto themselves by the changes $M \rightarrow -M$, $A_+ \rightarrow A_-$, $A_- \rightarrow A_+$, $z \rightarrow -z$, and $s \rightarrow s$. Second, note that the three asymptotic solutions as $|z| \rightarrow \infty$ are:

$$A_+ \sim e^{\frac{\gamma z}{1-M}} \quad s, A_- \sim \mathcal{O}\left(\frac{1}{z} e^{\frac{\gamma z}{1-M}}\right) \quad (29)$$

$$A_- \sim e^{\frac{-\gamma z}{1+M}} \quad s, A_+ \sim \mathcal{O}\left(\frac{1}{z} e^{\frac{-\gamma z}{1+M}}\right) \quad (30)$$

$$s \sim e^{\frac{-\gamma z}{M}} \quad A_+, A_- \sim \mathcal{O}\left(\frac{1}{z} e^{\frac{-\gamma z}{M}}\right). \quad (31)$$

If $M > 1$, there are no acceptable (decaying) asymptotic solutions as $z \rightarrow -\infty$ for $\mathbf{Re} \gamma > 0$. Thus, $M > 1$ has no unstable eigenmodes. Physically, this is because all solutions, even the upstream propagating Alfvén wave A_+ , are swept downstream.

Without flow, MHD stability equations are self-adjoint (Bernstein et. al. 1958) and γ^2 is real. With flow, no such property is known and γ^2 can be complex. However, in all our solution methods, γ^2 has been found to be real for this problem, although we have not been able to prove that this is rigorously true. The discrete positive real values for γ correspond to unstable growing modes, and the continuum along the imaginary γ axis represents traveling Alfvén waves.

In the following subsection, we present the numerical solution of equations (21)–(23). Various analytical limits that illuminate the numerical solutions are treated in subsection 3.2. An exactly soluble model with a straight magnetic field that demonstrates qualitatively

similar behavior is presented in subsection 3.3. Finally, in subsection 3.4, energy constraints on the instability are discussed.

3.1. Numerical Solutions

We looked for normal mode growth in the system defined by equations (21)–(23) using three different numerical methods. We directly solved for the eigenvalues γ of this system by matrix solution of the corresponding finite difference equations using the commercial numerical routine package LAPACK. We also found the eigenvalues of the equations to high precision using a 1-D shooting code in z driven by an adaptive step-size, fourth order Runge-Kutta method with fifth order correction (RK45). Finally, for equations (21)–(23) with γ replaced by $\partial/\partial t$, an initial-value code employing Barton’s method (Centrella and Wilson 1984) for second order accuracy in time was written to determine the fastest growing mode for any choice of parameters. Results from all three codes were consistent.

A stability diagram of unstable normal-mode growth rates and stable regions over the parameter space defined by M and s'_0 is presented in Figure 2. As we have already noted, no growing mode exists for $M > 1$. As well, it is obvious that for the non-positive values of the entropy gradient, $s'_0 \leq 0$, there can be no unstable mode growth since the atmosphere is stably or neutrally stratified; this is demonstrated by the energy arguments presented in section 3.4. Hence, Figure 2 need only cover the region of (M, s'_0) parameter space defined by $0 \leq M \leq 1$ and $s'_0 > 0$ to include all possible unstable mode growth.

Several features of Figure 2 are important to emphasize. First, for a system without plasma flow (along the line $M = 0$), we see that the entropy gradient must exceed a threshold value, $s'_0 > 1/4$, in order to become unstable when the fluid is supported by a shear magnetic field. Second, the qualitative effect of increasing the plasma flow (increasing M) on the instability growth rate depends on both the growth rate and the plasma flow. Away from marginal stability ($\gamma \geq 1$), an increase of the plasma flow—equivalent to moving along a horizontal line to the right on the stability diagram—decreases the instability growth rate as one may expect. Here, the growing perturbation is sheared out horizontally so that less gravitational potential energy is extracted by motions along the constant y' surface, reducing the instability growth rate. But near marginal stability ($\gamma < 1$), an increase in the shear flow effects the instability growth rate differently depending on the relative orders of the growth rate, γ , and of one minus the Alfvén Mach number, $1 - M$. The diagonal dotted line in Figure 2 denotes $\gamma = 1 - M$. In region (II) of the diagram, $\gamma > 1 - M$ and flow suppresses the instability. But, in region (I), where $\gamma < 1 - M$, an increase in the flow actually enhances the instability growth. This unexpected result can be explained with some physical insight. The

point where the instability can grow is localized at $z' = 0$ in our transformed coordinates; this is where the constant y' surface is vertical and motions along that surface can extract the most gravitational potential energy with which to drive the instability. When a shear plasma flow is introduced into the system, this is manifested in our transformed system by a plasma flow along the field lines in the $+z'$ direction. This causes the Alfvén modes in the $+z'$ and $-z'$ directions to propagate at different speeds in our transformed system. The counter-propagating mode (A_+ in our model) is slowed down, spending more time in the region around $z' = 0$ where unstable mode growth occurs. Hence, the instability is enhanced by a shear flow in the plasma. The final point to be gleaned from Figure 2 concerns the behavior as $M \rightarrow 1$, or as the Alfvén Mach number approaches one. In this region, every contour corresponding to a finite growth rate asymptotes to $s'_0 \rightarrow \infty$; hence, the instability is stabilized as the Alfvén Mach number approaches one.

3.2. Analytical Limits

The stability diagram, Figure 2, prominently displays the three main characteristics discussed in section 3.1: a threshold entropy gradient, $s'_0 > 1/4$, necessary for instability in the system without plasma flow; for increasing plasma flow, a reduction of the unstable growth away from marginal stability, but an enhancement of that unstable mode near marginal stability including a decrease in the threshold entropy gradient necessary for instability; and the stabilization of unstable normal modes as the Alfvén Mach number approaches one. Each of these characteristics is relevant in a different region of the (M, s'_0) parameter space of the diagram. By examining the model in each of these regions of parameter space, we can confirm and explain our results analytically.

First, we examine the criterion for instability in the absence of plasma flow in section 3.2.1; this corresponds to the left vertical axis of the stability diagram where $M = 0$. Next, in section 3.2.2, we conduct an asymptotic analysis in the $M \rightarrow 1$ limit—region (II) of the stability diagram—to show that the plasma is indeed stabilized as the Alfvénic Mach number approaches one. In section 3.2.3, we investigate the reduction of the threshold for instability with plasma flow; this covers the lower, right-hand side of region (I) of the stability diagram. A WKB analysis for a large instability growth rate, presented in section 3.2.4, yields the behavior of the system in the central and upper portion of the stability diagram; the suppression of the growth rate by flow in region (II) and its enhancement in region (I) are verified by the eigenvalue condition $\gamma(M, s'_0)$ obtained in this analysis.

3.2.1. Stability Criterion without Flow

Here we obtain the stability criterion for a magnetized fluid supported by a shear magnetic field in the Boussinesq limit with no shear flow. By using the substitution $v = \delta v_{\perp}/(1 + z^2)$, the equations without plasma flow ($M = 0$) can be simplified to a Sturm-Liouville equation of the form

$$\frac{d}{dz} \left[(1 + z^2) \frac{dv}{dz} \right] - [\gamma^2(1 + z^2) - s'_0] v = 0 \quad (32)$$

over the interval $(-\infty, +\infty)$. The boundary conditions on this system necessitate that $v \rightarrow 0$ as $z \rightarrow \pm\infty$. From Sturm's First Comparison Theorem (Ince 1926), we know that, as the eigenvalue γ^2 is increased, the solution will oscillate less rapidly with zeros of the function v leaving the interval $-\infty < z < \infty$ at the boundaries. Thus, if the solution with $\gamma^2 = 0$ oscillates, we can increase γ^2 until the boundary conditions are satisfied, so there will be an unstable solution. Note also that the fastest growing mode has no zeros in the interval and must be even in z .

Let $w(z)$ satisfy equation (32) with $\gamma^2 = 0$. Substituting a series solution of the form

$$w(z) = \sum_{n=0}^{\infty} a_n (1 + z^2)^{-(n+\alpha)}. \quad (33)$$

in equation (32) (with $\gamma^2 = 0$), we obtain the recurrence relation,

$$\frac{a_n}{a_{n-1}} = \frac{4(n + \alpha - 1)^2}{4(n + \alpha - 1/4)^2 + s'_0 - 1/4}, \quad (34)$$

with

$$\alpha = \frac{1}{4} \pm \frac{1}{4} \sqrt{1 - 4s'_0}. \quad (35)$$

When $s'_0 > 1/4$, solution (33) oscillates for $z \rightarrow \infty$, and clearly an unstable solution exists. Let us therefore consider stability when $s'_0 < 1/4$. We take the positive sign in equation (35); then w^2 is integrable for $z \rightarrow \infty$. We note that all a_n are positive if a_0 is positive. We choose $a_0 > 0$ such that $w > 0$. The series solution for $w(z)$ given by equation (33) is non-differentiable at $z = 0$ (as we see below). Thus, we cannot use the solution from equation (33) over the whole interval and must restrict its use to $z > 0$. Let us suppose (for contradiction) that there exists at least one unstable solution of equation (32). Further, let $v_0(z)$ be the most unstable solution—as noted above, $v_0(z)$ must be even in z and have no zeros in the interval $-\infty < z < \infty$. We therefore choose $v_0(z) > 0$ everywhere. It is straight forward to show that

$$v_0(0) \left. \frac{dw}{dz} \right|_{0+} = \gamma_0^2 \int_{0+}^{\infty} w v_0 (1 + z^2) dz, \quad (36)$$

where the limit 0^+ is infinitesimally above $z = 0$. Since the integral and v_0 in equation (36) are positive, we have stability, $\gamma_0^2 < 0$ (a contradiction), if $\frac{dw}{dz}|_{0^+} < 0$. Since every term in the series equation (33) is a monotonically decreasing function of z we expect $\frac{dw}{dz}|_{0^+} < 0$, but since the limit is nonuniform we take a more careful approach. We determine the sign of the limit $\frac{dw}{dz}|_{0^+}$ from an examination of the convergence of the series. It is straightforward to show that

$$a_n \sim \frac{A}{n^{3/2}} \quad (37)$$

as $n \rightarrow \infty$ with A a positive constant. Thus, the series for $w(z)$ (equation [33]) converges for $z \geq 0$. However, the series for $\frac{dw}{dz}$ converges for $z > 0$ but not for $z = 0$. Let us write for $z \rightarrow 0$

$$\frac{dw}{dz} = \sum_{n=0}^{\infty} \frac{-2z(n+\alpha)a_n}{(1+z^2)^{(n+\alpha+1)}} \simeq -Cz - 2 \sum_{n=N}^{\infty} \frac{Az n^{-1/2}}{(1+z^2)^n}, \quad (38)$$

where C is a positive constant and N is a large number in the range $1 \ll N \ll z^{-2}$. Using $(1+z^2)^{-n} \simeq e^{-nz^2}$, we obtain

$$\begin{aligned} \frac{dw}{dz} &\simeq -Cz - 2A \sum_{n=N}^{\infty} n^{-1/2} z e^{-nz^2} \simeq -Cz - 2A \int_N^{\infty} n^{-1/2} z e^{-nz^2} dn = -Cz - 2A \int_{\sqrt{N}z}^{\infty} e^{-p^2} dp \\ &\simeq -Cz - 2A \int_0^{\infty} e^{-p^2} dp = -Cz - A\sqrt{\pi}. \end{aligned} \quad (39)$$

Thus, the limit of $\frac{dw}{dz}$ as $z \rightarrow 0^+$ is $-\sqrt{\pi}A$, *i.e.* negative. From equation (36) we conclude that $\gamma_0^2 < 0$ and there are no unstable modes for $s'_0 < 1/4$. Thus, the necessary and sufficient condition for instability is $s'_0 > 1/4$.

This criterion can also be written

$$\frac{\rho'_0}{\rho_0} - \frac{p'_0}{\Gamma p_0} > \frac{1}{4} \frac{v_A^2}{gl_B^2}. \quad (40)$$

This confirms the result in Figure 2—that a threshold value of the entropy gradient, given by Equation (40), must be exceeded in order to cause instability when the fluid is supported by a shear magnetic field. Clearly, without magnetic shear ($l_B \rightarrow \infty$), the usual criterion, $s'_0 > 0$, holds and the motion is the simple interchange of field lines. With magnetic shear, the field lines *must* be bent since the interchange of field lines is impossible with finite displacements—thus magnetic shear is stabilizing.

3.2.2. Asymptotic Solution in the $M \rightarrow 1$ Limit

An asymptotic, boundary layer analysis can be carried out in the limit that $M \rightarrow 1$. This asymptotic expansion is described in Appendix B. The eigenvalue condition derived

for this limit in that appendix is

$$\gamma^2 \simeq s'_0(1 - M^2).$$

This relation explains the upturn towards infinity of the constant growth rate contours in region (II) of Figure 2 as $M \rightarrow 1$.

3.2.3. Solution in the $\gamma \rightarrow 0$, $M \rightarrow 1$ Limit

We demonstrate that the threshold entropy gradient for instability (the limit that $\gamma \rightarrow 0$) decreases as the plasma flow velocity is increased and that the threshold value of s'_0 approaches zero linearly as $M \rightarrow 1$. Letting $1 - M \sim \epsilon$, we can redefine the following variables in terms of ϵ : $\gamma = \epsilon\bar{\gamma}$, $A_- = \epsilon\bar{A}_-$, $s = \epsilon\bar{s}$ and $s'_0 = \epsilon\bar{s}'_0$. For $M \rightarrow 1$, we can drop terms of order ϵ^2 and cancel ϵ from each remaining term to yield the simplified set of equations

$$-\frac{dA_+}{dz} = -\bar{\gamma}A_+ + 2\frac{z}{1+z^2}\bar{A}_- - \frac{\bar{s}}{(1+z^2)^{1/2}} \quad (41a)$$

$$2\frac{d\bar{A}_-}{dz} = -\frac{z}{1+z^2}A_+ + \frac{\bar{s}}{(1+z^2)^{1/2}} \quad (41b)$$

$$\frac{d\bar{s}}{dz} = -\frac{1}{2}\frac{A_+}{(1+z^2)^{1/2}}\bar{s}'_0. \quad (41c)$$

These equations are now independent of ϵ , or, equivalently, are independent of M . The equations will hold true for constant values of $\bar{\gamma}$ and \bar{s}'_0 . In this case, if we have a negligibly small value $\bar{\gamma} \rightarrow 0$, we obtain the corresponding threshold value of $s'_0 = \bar{s}'_0(1 - M)$, where \bar{s}'_0 is a constant. Thus, the threshold entropy gradient for stability must linearly approach zero as $M \rightarrow 1$, as seen in the lower right-hand corner of Figure 2.

3.2.4. WKB Analysis

A complete solution of the model for a large growth rate γ can be constructed if we assume an ordering, for a small parameter ϵ , such that $\gamma \sim \mathcal{O}(\epsilon^{-1})$, $\frac{d}{dz} \sim \mathcal{O}(\epsilon^{-1})$, $s \sim \mathcal{O}(\epsilon^{-1})$, and $s'_0 \sim \mathcal{O}(\epsilon^{-2})$. In this case, we can neglect the second term on the right hand side of both equations (21) and (22). Converting back from Elsässer variables to δB_\perp and δv_\perp notation, combining the three equations into a single second order equation, and neglecting the term $M s \frac{d}{dz} \left(\frac{1}{(1+z^2)^{1/2}} \right)$ (which can be shown to be small), yields

$$(1 - M^2)\frac{d^2\delta v_\perp}{dz^2} - 2\gamma M\frac{d\delta v_\perp}{dz} - \left[\gamma^2 - \frac{s'_0}{1+z^2} \right] \delta v_\perp = 0. \quad (42)$$

Changing variables with an integrating factor to $v = \exp\left(\frac{\gamma M z}{1-M^2}\right) \delta v_{\perp}$, we obtain

$$\frac{d^2 v}{dz^2} - \frac{1}{(1-M^2)^2} \left[\gamma^2 - \frac{s'_0(1-M^2)}{1+z^2} \right] v = 0. \quad (43)$$

We assume a WKB solution of the form $e^{i \int k(z) dz}$ and find

$$v = \bar{v} \exp \left(\pm \frac{i}{1-M^2} \int^z \left[\frac{s'_0(1-M^2)}{1+z'^2} - \gamma^2 \right]^{1/2} dz' \right). \quad (44)$$

The turning points are at $z = \pm z_0$ where

$$z_0^2 = \frac{s'_0(1-M^2)}{\gamma^2} - 1. \quad (45)$$

For $|z| > z_0$, the WKB solutions are decaying exponentials; in the region $-z_0 < z < z_0$, the WKB solution is an oscillatory function.

In the usual way (Bender and Orszag 1978), we obtain the Bohr-Sommerfeld quantization condition

$$\int_{-z_0}^{z_0} \left[\frac{s'_0(1-M^2)}{1+z^2} - \gamma^2 \right]^{1/2} dz = 2n\pi(1-M^2). \quad (46)$$

The growth rate of the n th mode is then given, for small z_0 , by

$$\gamma^2 = [s'_0 - 2n(s'_0)^{1/2}(1-M^2)^{1/2}] (1-M^2). \quad (47)$$

For a large growth rate $\gamma \sim \mathcal{O}(\epsilon^{-1})$ and the lowest, nontrivial eigenmode $n = 1$, we can solve this eigenvalue condition for s'_0 to obtain

$$s'_0 = \frac{\gamma^2}{1-M^2} + 2\gamma. \quad (48)$$

This condition agrees with the behavior of the constant growth rate contours in region (II) of Figure 2. Although we do not expect the eigenvalue condition in the WKB approximation to be precise in the limit of small growth rate, $\gamma \sim \mathcal{O}(\epsilon)$, we do find to lowest order the qualitatively correct form,

$$s'_0 \sim 1 - M^2, \quad (49)$$

that the contours in region (I) decrease like $1 - M^2$.

3.3. Bounded, Straight-Field Case

The general model defined by this paper has the characteristic that the shear in the magnetic field localizes the region of instability around where the constant y' surface is vertical (this corresponds to $z' = 0$ in our transformed coordinate system). With this characteristic as our guide, an exactly soluble, simplified model can be constructed which demonstrates the same qualitative behavior displayed in Figure 2. We construct a case with a straight magnetic field and a plasma flow along the field lines which has boundaries at $z = \pm L$. Since the explicit z dependence drops out of the equations in the straight-field limit ($l_B \rightarrow \infty$), we Fourier transform in z to obtain the algebraic dispersion relation

$$(\gamma + iMk_z) [(1 - M^2)k_z^2 + 2i\gamma Mk_z + \gamma^2 - s'_0] = 0. \quad (50)$$

If we remove the plasma flow from the system by setting $M = 0$, this dispersion relation agrees with the results of Newcomb (1961) for a straight-field without flow in the Boussinesq limit.

We solve for the three solutions for k_z from equation (50) and find the eigenvectors corresponding to each k_z . Constructing general solutions for δB_\perp , δv_\perp , and s from these eigenvectors, we find the eigenvalue condition $\gamma(M, s'_0)$ that must hold in order to satisfy the three necessary boundary conditions on the system. The boundary conditions we apply are $\delta v_\perp = 0$ at $z = \pm L$ and the upstream boundary condition $s = 0$ at $z = -L$. The eigenvalue condition thus obtained is

$$\gamma^2 = \left[s'_0 - \left(\frac{n\pi}{2L} \right)^2 (1 - M^2) \right] (1 - M^2) \quad (51)$$

for the n th order unstable mode where $n = 1, 2, 3, \dots$

A plot of constant γ contours is displayed in Figure 3. Note that the qualitative behavior pointed out in the text in section 3.1 is demonstrated by this simplified model. Therefore, the magnetic shear is not responsible for the unexpected decrease in the stability threshold with shear flow; only a localization of the instability is necessary to demonstrate this characteristic. A quantitative comparison of Figures 2 and 3 shows that, to yield equivalent growth rates, a much larger entropy gradient must be supplied in the unbounded case with magnetic shear than in the bounded, straight-field model. We can understand the difference as follows. The energy required to bend the magnetic field lines slows the growth of the instability. In the bounded case, this energy is needed to bend the field line only within the bounded domain. But, in the unbounded model, the bending of the field lines occurs over a larger extent in z , thus requiring more energy and so more effectively suppressing the instability.

3.4. Energy Conservation

In the standard way, equations (21)–(23) can be combined, replacing γ with the time derivative $\frac{\partial}{\partial t}$, to obtain an energy integral for the model. Converting back to δv_{\perp} and δB_{\perp} using equations (24) and (25), we find

$$\frac{\partial}{\partial t} \left\{ \frac{1}{2} \int_{-\infty}^{\infty} \left[\frac{\delta B_{\perp}^2 + \delta v_{\perp}^2}{1 + z^2} - \frac{2M\delta B_{\perp}\delta v_{\perp}}{1 + z^2} - \frac{s^2}{s'_0} \right] dz \right\} = M \int_{-\infty}^{\infty} \frac{s\delta B_{\perp}}{1 + z^2} dz. \quad (52)$$

Adopting the terminology of Hayashi and Young (1987), we define the integral on the left-hand side of equation (52) as the wave energy of the perturbation. Note that, in the absence of flow ($M = 0$), the wave energy is constant in time. Equation (52) supplies a limit on the value of s'_0 necessary for instability: since the δB_{\perp}^2 and δv_{\perp}^2 terms are both positive definite, an instability can only develop for $s'_0 > 0$. In this case, gravitational potential energy from the s^2 term can be harnessed to drive the kinetic energy and field line bending of the instability.

By the same method as above, we find that the wave energy integral for the straight-field model bounded at $z = \pm L$, in section 3.3, has the form

$$\frac{\partial}{\partial t} \left\{ \frac{1}{2} \int_{-L}^L \left[\delta B_{\perp}^2 + \delta v_{\perp}^2 - \frac{s^2}{s'_0} \right] dz \right\} = \frac{M}{2} \left\{ \delta B_{\perp}^2(-L) - \delta B_{\perp}^2(L) + \frac{s^2(L)}{s'_0} \right\}. \quad (53)$$

Without flow, again, we find that the necessary condition for instability to develop is $s'_0 > 0$ and that the wave energy integral is constant in time. In the presence of flow, we interpret the terms on the right-hand side of equation (53) as follows: $\delta B_{\perp}^2(-L)$ represents the flow of magnetic energy into the region, $-\delta B_{\perp}^2(L)$ represents the flow of magnetic energy out of the region, and $\frac{s^2(L)}{s'_0}$ represents the flow of gravitational potential energy out of the the region.

4. Discussion

To study the effect of magnetic shear and shear flow on local gravitationally induced instabilities, we have constructed a simple model in the Boussinesq limit of ideal MHD. Numerical solutions to this model yield a stability diagram of the (M, s'_0) parameter space. This stability diagram has three important characteristics. First, there exists a threshold entropy gradient for unstable mode growth, demonstrating that magnetic shear is a stabilizing influence. Second, flow serves to suppress mode growth in a substantially unstable regime, but near marginal stability it lessens the stabilizing effect of magnetic shear, enhancing unstable mode growth rates and lowering the threshold entropy gradient necessary for instability. Third, normal modes of instability are stabilized completely as the Alfvén Mach

number approaches one because the disturbance is swept downstream out of the unstable region. Analytical work corroborates these characteristics in the different regions of (M, s'_0) parameter space.

In a shear magnetic field without flow, the characteristic shape of the unstable mode is such that the field lines remain on the constant y' surface shown in Figure 1; hence, in the lab frame, the field lines must twist as they fall under gravity to remain on this surface. This occurs because the perturbed field line at any vertical height x must align with the direction of the unperturbed field at that height to facilitate interchange. Unlike the ordinary interchange of straight field lines, if magnetic shear is present, the field line *must* be bent to allow interchange; this is the root of the stabilizing influence of the shear magnetic field. Energy extracted from gravitational potential energy as the field line falls must supply both the kinetic energy of the moving plasma, which is frozen to the field line, and the energy required to bend the field line. Unstable motions are localized about the point where the constant y' surface is vertical ($z = 0$ in Figure 1), because this point is where motions on that surface extract the most gravitational potential energy while minimizing field line bending. When plasma shear flow is included in the problem, this unstable region moves in the lab frame with the flow velocity v_f in the $-\hat{z}$ direction. Therefore, this characteristic twisting geometry propagates along z at a speed $v_f = v_0 \frac{l_B}{l_v}$ determined by the local flow speed v_0 , flow shear length l_v , and magnetic field shear length l_B . Typical eigenfunctions for an entropy gradient of $s'_0 = 0.6$ and Alfvén Mach numbers $M = 0$ and $M = 0.8$ are displayed in Figure 4.

The modifications of the gravitational stability of a magnetized plasma due to the presence of magnetic shear and shear flow impact several diverse subjects. In solar physics, one of the key processes necessary for the success of the interface dynamo (Parker 1993; Charbonneau and MacGregor 1996) is the storage of an intense toroidal field in the solar tachocline (Spiegel and Zahn 1992) until an instability causes an isolated flux tube to rise into the base of the convection zone (Adam 1978; Cally 1983; Cally and Adam 1983; Hughes and Cattaneo 1987; Cattaneo and Hughes 1988; Cattaneo et. al. 1990; Schussler et. al. 1994; Caligari et. al. 1995; Gilman and Fox 1997; Barnes et. al. 1998). Shear flow is present due to the large differential rotation of the sun in the tachocline region (Thompson 1996; Schou et. al. 1998), and some magnetic shear probably exists here as well; the impact of shear flow and magnetic shear may alter gravitational stability within this region. There are two regions in galactic physics where the conditions in our model may apply: near the center of the galaxy, where there likely exists a region of magnetic shear in which the large-scale magnetic field changes from primarily azimuthal to primarily vertical (Zweibel and Heiles 1997) and shear flow is present through differential rotation, and in the disk of the galaxy, where both magnetic shear and shear flow may be present in the vertical direction away

from the mid-plane. In examining the mechanisms for turbulence in accretion disks, Balbus and Hawley (1991) pointed out that a previously discovered (Velikhov 1959; Chandrasekhar 1960, 1961) but unappreciated linear MHD instability, driven by differential rotation coupled with magnetic tension, would occur if the accretion disk were threaded by a weak magnetic field. But the Balbus-Hawley instability bends the magnetic field lines extensively; thus, it is stabilized by magnetic tension for large magnetic field strengths (Blaes and Balbus 1994; Urpin 1996; Kitchatinov and Rüdiger 1997). Although the twisting interchange instability studied here depends not on rotation but on an entropy gradient, it has a characteristic geometry that minimizes field line bending and so may be important in regions of large field strength. As is well known within the fusion community (Roberts and Taylor 1965), employing a sheared toroidal magnetic field in a tokamak can help to stabilize, or at least suppress, ballooning instabilities (buoyant interchange instabilities driven by pressure and curvature forces). The idea of employing shear flow to further stabilize ballooning instabilities has gained much attention in the past decade (Waelbroeck and Chen 1991; Hassam 1991, 1996, 1999; Miller et. al. 1995). Our work demonstrates that, near marginal stability, shear flow actually lessens the stabilizing effect of magnetic shear, lowering the threshold entropy gradient required for instability and enhancing the unstable mode growth rate. Full stabilization of the plasma will occur only if the Alfvén Mach number of the plasma flow (as defined in our transformed coordinates) exceeds one. The local nature of the instability examined in this work means that our treatment may apply locally in more complicated environments. The instability may behave as a traveling “wave packet” which moves with the intersection of shear magnetic field lines (where the constant y' surface is vertical); the disturbance may move in and out of unstable regions, with the perturbation growing where conditions are unstable and decaying in stable regions.

We have extended the model to include compressibility. In this case, the behavior is governed by a system of five coupled, first-order ordinary differential equations. Five parameters are necessary to describe the system: the Alfvén Mach number, the plasma β , the density gradient, the pressure gradient, and the magnetic field gradient. Over some portions of this five-dimensional parameter space, the growth rate eigenvalue γ does indeed become complex. Producing a simple answer from this more complicated model is quite difficult. Our current research is addressing this difficulty. But, the magnetic-buoyancy instability (Parker 1979), which depends on compressibility, cannot be investigated without employing this more detailed treatment. We will then be able to relate our work quantitatively to applications such as the stability of magnetic fields in the solar tachocline. One final possible extension of this research is an investigation of the nonlinear behavior using an initial-value code.

The research was performed under appointment of Greg Howes to the Fusion Energy

Sciences Fellowship program administered by the Oak Ridge Institute for Science and Education under a contract between the U.S. Department of Energy and the Oak Ridge Associated Universities. It was supported in part by the National Science Foundation under Grant No. PHY94-07194. We are grateful to B. Albright, A. Cumming, B. Dorland, E. Quataert, S. Tobias, J. Toomre, and E. Zweibel for useful discussions.

A. Twisting Modes vs. Fourier Modes

In the sheared magnetic field, the local unstable modes can be written in two ways (Roberts and Taylor 1965); we call them twisting and Fourier modes. For the reader's convenience, we summarize the essence of the argument here. In the twisted field line coordinates, we obtain the twisted mode where a perturbed quantity $\Phi(x, y, z, t)$ is given by

$$\Phi_T = \overline{\Phi}_T(z, x)e^{iky'+\gamma t} = \overline{\Phi}_T(z, x)e^{iky-ik\frac{xz}{l_B}+\gamma t} \quad (\text{A1})$$

with $\overline{\Phi}_T$ localized in z and varying weakly in x compared to k^{-1} . But since the origin in z is arbitrary, we can also write

$$\Phi'_T = \overline{\Phi}_T(z - z_0, x)e^{iky-ik\frac{x(z-z_0)}{l_B}+\gamma t}. \quad (\text{A2})$$

Thus, there are an infinite number of twisting modes, each with a different origin of the twist. We can construct a mode that does not depend on z —a Fourier mode—by integrating equation (A2) over z_0

$$\Phi_F = \int_{-\infty}^{\infty} \Phi'_T(z - z_0, x, y, t)dz_0 = \overline{\Phi}_F\left(\frac{kx}{l_B}, x\right)e^{iky+\gamma t}, \quad (\text{A3})$$

where

$$\overline{\Phi}_F\left(\frac{kx}{l_B}, x\right) = \int_{-\infty}^{\infty} \overline{\Phi}_T(z', x)e^{-i\frac{kx}{l_B}z'dz'}. \quad (\text{A4})$$

Thus, the Fourier modes and the twisting modes are related by a Fourier transform. Clearly, the Fourier mode can be made by “adding” twisting modes together (equation [A3]), or vice versa, using the Fourier inversion theorem on equation (A4); see Cowley et. al. (1991) for pictures of this superposition. The Fourier modes are narrowly localized in x —typically $\Delta x \sim \frac{\Delta x}{k\Delta z}$ where Δx is the x width of the Fourier mode and Δz is the z width of the twisting mode. Note this x localization of the Fourier mode is narrow compared to the x variation of the twisting mode. In this paper, we have taken the twisting mode representation for two reasons: first, the role of the flow, we believe, is more intuitive in this picture; and, second, the twisting modes are finite in z extent and therefore represent more easily the evolution of an initial value problem.

B. Asymptotic Analysis as $M \rightarrow 1$

To demonstrate stabilization as the Alfvén Mach number approaches one, as seen of region (II) of Figure 2, we perform an asymptotic analysis of our model in the limit $M \rightarrow 1$. For a small dimensionless parameter ϵ , we quantify the order of this limit as $1 - M \sim \mathcal{O}(\epsilon^2)$. We expect the instability growth rate to be $\gamma \sim \mathcal{O}(\epsilon)$. Identifying the terms in the dimensionless system of equations (21)–(23) for reference, we have

$$\begin{aligned}
 -(1 - M) \frac{dA_+}{dz} &= -\gamma A_+ & +(1 + M) \frac{z}{1+z^2} A_- & - \frac{s}{(1+z^2)^{1/2}} \\
 (1) & & (2) & & (3) & & (4)
 \end{aligned} \tag{B1}$$

$$\begin{aligned}
 (1 + M) \frac{dA_-}{dz} &= -\gamma A_- & -(1 - M) \frac{z}{1+z^2} A_+ & + \frac{s}{(1+z^2)^{1/2}} \\
 (5) & & (6) & & (7) & & (8)
 \end{aligned} \tag{B2}$$

$$\begin{aligned}
 M \frac{ds}{dz} &= -\gamma s & - \frac{s'_0}{2} \frac{A_+}{(1+z^2)^{1/2}} & + \frac{s'_0}{2} \frac{A_-}{(1+z^2)^{1/2}}. \\
 (9) & & (10) & & (11) & & (12)
 \end{aligned} \tag{B3}$$

The boundary conditions demand $A_+, A_-, s \rightarrow 0$ as $|z| \rightarrow \infty$. Asymptotic solutions in the $M \rightarrow 1$ limit can be found in the four regions along z displayed in Figure 5. Below we find the solutions for each of these regions and, by matching the solutions between these regions, we obtain an eigenvalue condition on the growth rate demonstrating stabilization as the Alfvén Mach number approaches one. First, we obtain two reductions of equations (B1)–(B3); one over a boundary layer where $|z| \ll \epsilon^{-1}$, and the other over an outer region where $|z| \gg 1$. Then, we present the solutions in each of the four regions in Figure 5.

As the Alfvén Mach number approaches one, regions (1), (2), and (3) of Figure 5 behave like a boundary layer region: we expect derivatives to be large and thus take $\frac{d}{dz} \sim \mathcal{O}(\epsilon^{-1})$. We treat $z \sim \mathcal{O}(1)$ over these three regions. Balance of the dominant terms (9) and (11) in equation (B3) shows that $s \sim \mathcal{O}(\epsilon A_+)$. In turn, this demands that terms (5) and (8) must balance in equation (B2), yielding the ordering $A_- \sim \mathcal{O}(\epsilon^2 A_+)$. Adopting the specified ordering allows us to drop terms (6), (7), (10), and (12) from equations (B1)–(B3); term (3), although one order in ϵ smaller than the other terms in equation (B1), will contribute in the regions for $z > 1$, so we retain it in order to be certain that our first order correction in region (3) is valid. The remaining equations can be combined to a single third-order equation in A_- and simplified by the substitution $z = \sinh \theta$ to obtain

$$\frac{2M(1 - M)}{s'_0} \frac{d^3 A_-}{d\theta^3} - \frac{2\gamma M}{s'_0} \cosh \theta \frac{d^2 A_-}{d\theta^2} + \frac{dA_-}{d\theta} - \tanh \theta A_- = 0. \tag{B4}$$

In region (4), we find the smoothly varying outer solution over which $z \sim \mathcal{O}(\epsilon^{-1})$. We expect that $\frac{d}{dz} \sim \mathcal{O}(\epsilon)$ here. By insisting that terms (9) and (10) balance with term (11)

in equation (B3), we find that $s \sim \mathcal{O}(A_+)$. Similarly, by balancing terms (5) and (6) with term (8) in equation (B2), we obtain $A_- \sim \mathcal{O}(A_+)$. This ordering allows us to drop terms (1) and (7) in equations (B1)–(B3). Approximating $(1+z^2)^{1/2} \simeq z$, substituting $A_- = zB_-$, and combining the equations, we obtain the second-order equation

$$M(1+M)z^2 \frac{d^2 B_-}{dz^2} + \left[(1+2M)\gamma z^2 + 3M(1+M)z - \frac{(1+M)s'_0}{2\gamma} \right] \frac{dB_-}{dz} + [\gamma^2 z^2 + (1+3M)\gamma z + M(1+M) - s'_0] B_- = 0. \quad (\text{B5})$$

To find the solution in region (1), we assume an eikonal solution for equation (B4). Neglecting the trivial constant solution, we find two independent solutions of the form

$$A_- \sim \frac{1}{(1+z^2)^{3/4} [(1+z^2)^{1/2} + z]^{1/2}} \exp\left(\frac{\gamma}{2(1-M)} [z + (1+z^2)^{1/2}]\right) \quad (\text{B6})$$

$$A_- \sim \frac{z + (1+z^2)^{1/2}}{(1+z^2)^{1/2}} \exp\left(\frac{\gamma}{2(1-M)} [z - (1+z^2)^{1/2}] + z [z - (1+z^2)^{1/2}]\right). \quad (\text{B7})$$

To get the behavior for $|z| \gg 1$, we can expand $(1+z^2)^{1/2} \simeq |z| + 1/2|z|$. For region (1), we note that $z < 0$ and, retaining only the dominant terms, we obtain solutions of the form

$$A_- \sim \frac{1}{z} \exp\left(\frac{-\gamma}{4(1-M)z}\right) \quad (\text{B8})$$

$$A_- \sim \frac{1}{z^2} \exp\left(\frac{\gamma z}{1-M}\right). \quad (\text{B9})$$

The boundary conditions impose that $A_- \rightarrow 0$ as $z \rightarrow -\infty$, so our solution in region (1) must be entirely of the form of equation (B9), a growing solution in the $+z$ direction. To determine the behavior of equations (B6) and (B7) in the overlap with region (2), we take the limit $|z| \ll 1$ and approximate $(1+z^2)^{1/2} \simeq 1 + z^2/2$ to get the two solutions

$$A_- \sim \exp\left(\frac{\gamma}{2(1-M)} [z + z^2/2]\right) \quad (\text{B10})$$

$$A_- \sim \exp\left(\frac{\gamma}{2(1-M)} [z - z^2/2]\right). \quad (\text{B11})$$

One of these solutions must smoothly match onto the solution for region (2).

Region (1)'s solution will be valid as we move in the $+z$ direction until the eikonal approximation, $\frac{\gamma z}{1-M} \gg 1$, breaks down. The failure of this condition occurs in region (2) of Figure 5 where $z \sim \mathcal{O}(\epsilon)$. For region (2), we expand equation (B4) about $z = 0$. For $z \ll 1$, $\cosh \theta \simeq 1$ and $\tanh \theta \simeq \theta$ where $\theta \ll 1$, so we can drop the last term of equation (B4).

Letting $f = \frac{dA_-}{d\theta}$ and using the integrating factor $f = B_- \exp\left(\frac{\gamma \sinh \theta}{2(1-M)}\right)$ to simplify the result, we obtain the equation

$$\frac{d^2 B_-}{d\theta^2} - \left[\frac{\gamma^2 \cosh^2 \theta}{4(1-M)^2} - \frac{\gamma \sinh \theta}{2(1-M)} - \frac{s'_0}{2M(1-M)} \right] B_- = 0. \quad (\text{B12})$$

Neglecting the central term in the coefficient of B_- because it is an order ϵ smaller than the other terms, we can cast equation (B12) in the form of Hermite's equation for which the solutions are well known. Therefore, for the $n = 0$ Hermite polynomial, the solution in region (2) is

$$A_- \sim \int^z \exp\left(\frac{\gamma}{2(1-M)}(z' - z'^2/2)\right) dz', \quad (\text{B13})$$

and the eigenvalue condition on the growth rate imposed by Hermite's equation is

$$\gamma^2 = \frac{2s'_0(1-M)}{M} - 2(2n+1)\gamma(1-M) \quad (\text{B14})$$

for the n th Hermite polynomial. Thus, we find that the solution in region (1) given by equation (B11) matches smoothly onto our solution in region (2).

In region (3), we once again assume an eikonal solution for equation (B4) and find the two solutions given by equations (B6) and (B7). To match with region (2), find the $|z| \ll 1$ limit of these equations, yielding once more equations (B10) and (B11); we observe that equation (B11) for the small z limit of region (3) matches solution (B13) for region (2). In the $|z| \gg 1$ limit of equations (B6) and (B7) for region (3), we obtain the solutions (for $z > 0$)

$$A_- \sim \frac{1}{z^2} \exp\left(\frac{\gamma z}{1-M}\right) \quad (\text{B15})$$

$$A_- \sim \exp\left(\frac{-\gamma}{4(1-M)z}\right). \quad (\text{B16})$$

To continue our asymptotic solution, we must smoothly match one of these region (3) solutions to the solution for region (4) in the overlap around $z \sim \mathcal{O}(\epsilon^{-1/2})$.

In region (4), we assume eikonal solutions for equation (B5) in the limit $z \rightarrow 0$. The two solutions found are

$$A_- \sim z \quad (\text{B17})$$

$$A_- \sim \exp\left(\frac{-s'_0}{2\gamma M z}\right). \quad (\text{B18})$$

Hence, we can match the solution given by equation (B16) in region (3) with the solution given by equation (B18) in region (4) if

$$\frac{\gamma}{4(1-M)} = \frac{s'_0}{2\gamma M}. \quad (\text{B19})$$

But, this is identical to the lowest order of the eigenvalue condition, equation (B14). To complete our asymptotic solution, we must find that a solution to equation (B5) in the limit $z \rightarrow \infty$ which satisfies the boundary condition that $A_- \rightarrow 0$ as $z \rightarrow \infty$. In this limit, the two solutions take the form

$$A_- \sim \exp\left(\frac{-\gamma z}{M}\right) \quad (\text{B20})$$

$$A_- \sim \exp\left(\frac{-\gamma z}{1+M}\right). \quad (\text{B21})$$

Both of these solutions satisfy the boundary condition as $z \rightarrow \infty$.

Now that we have seen that it is possible to construct a complete asymptotic solution in the limit $M \rightarrow 1$, let us examine this solution more closely. Beginning in region (1) at the left of Figure 5, the boundary conditions demand that the solution must be solely of the form of equation (B9). But, as behavior in regions (1), (2), and (3) is governed by equation (B4), the eikonal approximation must break down in region (2) in order for the solution in region (1) to convert to the solution given by equation (B16) in region (3) so that smooth matching may be accomplished with solution (B18) in region (4). The failure of the eikonal approximation around $z = 0$ yields a reduction of equation (B4) to the Hermite-type equation (B12). The requirement that a solution to this equation exist imposes the eigenvalue condition, equation (B14). This single condition can also be used to smoothly match solution (B16) in region (3) to solution (B18) in region (4). Finally, region (4) is governed by equation (B5). In the limit $z \rightarrow 0$, this equation yields a matching solution in the overlap with region (3); and, in the limit $z \rightarrow \infty$, it provides two solutions which both satisfy the boundary conditions as $z \rightarrow \infty$. Therefore, the single condition necessary to find a smooth solution which satisfies the boundary conditions is the eigenvalue condition, equation (B14). To lowest order, this condition can be written in a more recognizable form in the limit $M \rightarrow 1$ as

$$\gamma^2 \simeq s'_0(1 - M^2). \quad (\text{B22})$$

Thus, in region (II) of Figure 2, where $\gamma \gg 1 - M$, the behavior is clearly demonstrated—that stabilization occurs as the Alfvén Mach number approaches one.

REFERENCES

- Adam, J. A. 1978, *J. Plasma Phys.*, 19, 77.
- Balbus, S. A. and Hawley, J. F. 1991, *ApJ*, 376, 214.
- Barnes, G., MacGregor, K. B., and Charbonneau, P. 1998, *ApJ*, 498, L169.

- Bender, C. M. and Orszag, S. A. 1978, *Advanced Mathematical Methods for Scientists and Engineers*, New York: McGraw-Hill.
- Bernstein, I. B., Frieman, E. A., Kruskal, M. D., and Kulsrud, R. M. 1958, *Proc. Roy. Soc.*, A244, 17.
- Blaes, O. M. and Balbus, S. A. 1994, *ApJ*, 421, 163.
- Caligari, P., Moreno-Insertis, F. and Schussler, M. 1995, *ApJ*, 441, 886.
- Cally, P. S. 1983, *Geophys. Astrophys. Fluid Dynamics*, 23, 43.
- Cally, P. S. and Adam, J. A. 1983, *Geophys. Astrophys. Fluid Dynamics*, 23, 57.
- Cattaneo, F. and Hughes, D.W. 1988, *J. Fluid Mech.*, 196, 323.
- Cattaneo, F., Chiueh, T., and Hughes, D.W. 1990, *J. Fluid Mech.*, 219, 1.
- Centrella, J. and Wilson, J. R. 1984, *ApJS*, 54, 229.
- Chandrasekhar, S. 1960, *Proc. Natl. Acad. Sci.*, 46, 253.
- Chandrasekhar, S. 1961, *Hydrodynamic and Hydromagnetic Stability*, Oxford: Oxford Univ. Press.
- Charbonneau, P. and MacGregor, K. B. 1997, *ApJ*, 473, L59.
- Cowley, S. C., Kulsrud, R.M. and Sudan, R. 1991, *Phys. Fluids B*, 3, 2767.
- Gilman, P. A. and Fox P. A. 1997, *ApJ*, 484, 439.
- Goldreich, P. and Lynden-Bell, D. 1965, *MNRAS*, 130, 125.
- Hassam, A. B. 1991, *Comments Plasma Phys. and Controlled Fusion*, 14, 275.
- Hassam, A. B. 1996, *Nuclear Fusion*, 36, 707.
- Hassam, A. B. 1999, *Phys. Plasmas*, 6, 3772.
- Hayashi, Y.-Y. and Young, W. R. 1987, *J. Fluid Mech.*, 184, 477.
- Hughes, D.W. and Cattaneo, F. 1987, *Geophys. Astrophys. Fluid Dynamics*, 39, 65.
- Ince, E. L. 1926, *Ordinary Differential Equations*, New York: Dover.
- Kitchatinov, L. and Rüdiger, G. 1997, *MNRAS*, 286, 757.

- Miller, R. L., Waelbroeck, F. L., Hassam, A. B., and Waltz, R. E. 1995, *Phys. Plasmas*, 2, 3676.
- Newcomb, W. A. 1961, *Phys. Fluids*, 4, 391.
- Parker, E. N. 1979, *Cosmical Magnetic Fields: Their Origin and thier Activity*, Oxford: Clarendon Press.
- Parker, E. N. 1993, *ApJ*, 408, 707.
- Roberts, K. V. and Taylor, J. B. 1965, *Phys. Fluids*, 8, 315.
- Schou, J. et. al. 1998, *ApJ*, 505, 390.
- Schussler, M., Caligari, P., Ferriz-Mas, A. and Moreno-Insertis, F. 1994, *Astron. Astrophys.*, 281, L69.
- Schwarzschild, K. 1906, *Nachr. Kgl. Ges. Wiss. Göttingen*, p. 41.
- Spiegel, E. A. and Zahn, J.-P. 1992, *Astron. Astrophys.*, 265, 106.
- Thompson, M. J. et. al. 1996, *Science*, 272, 1300.
- Urpin, V. 1996, *MNRAS*, 280, 149.
- Velikhov, E. P. 1959, *Sov. Phys. JETP*, 36, 995.
- Waelbroeck, F. L., and Chen, L. 1991, *Phys. Fluids B*, 3, 601.
- Zweibel, E. G., and Heiles, C. 1997, *Nature*, 385, 131.

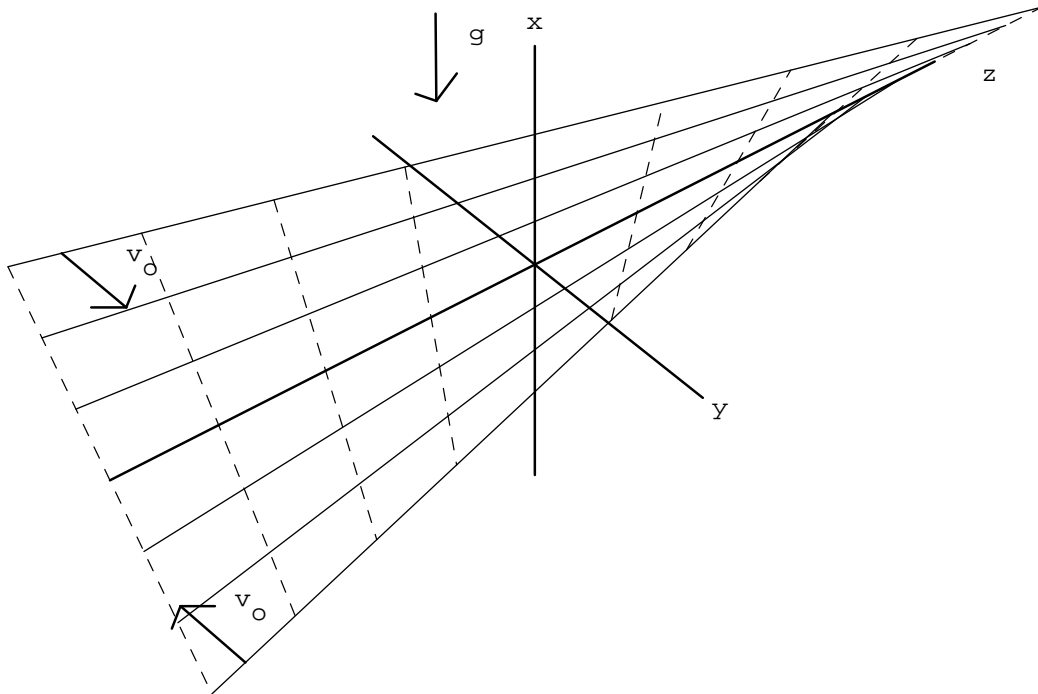


Fig. 1.— The geometry of the shear magnetic field as well as the applied shear flow (shown as v_0) is shown. The constant y' surface is represented by the magnetic field lines (solid lines) and the dashed lines.

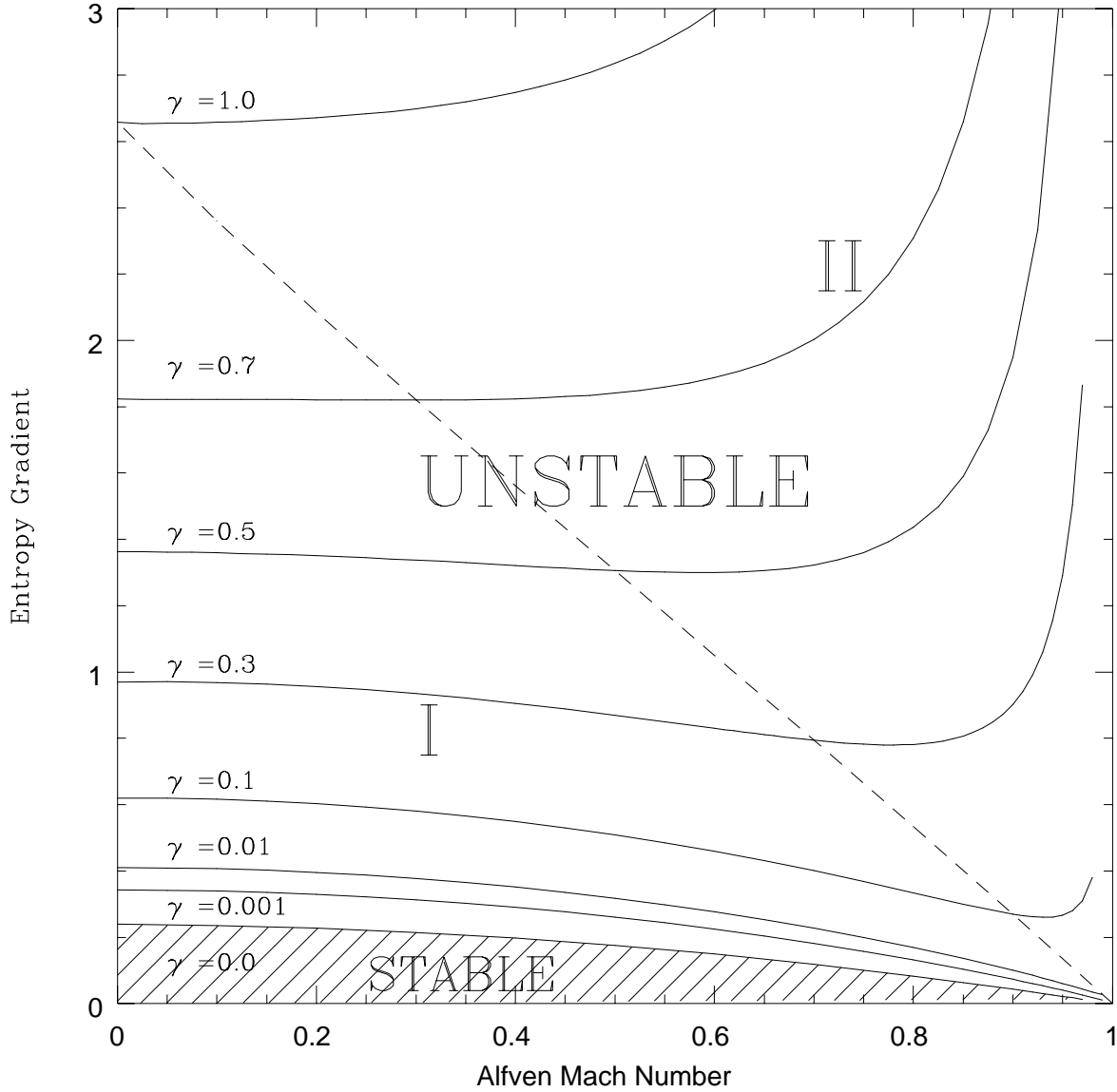


Fig. 2.— Stability diagram for the Boussinesq limit: Contours of constant normalized growth rate γ are plotted over the space of entropy gradient s'_0 vs. Alfvén Mach number M . The stable parameter regime is denoted by hashing. The diagonal dotted line denotes $\gamma = 1 - M$, separating unstable region (I), where flow enhances instability growth, from unstable region (II), where flow suppresses the instability.

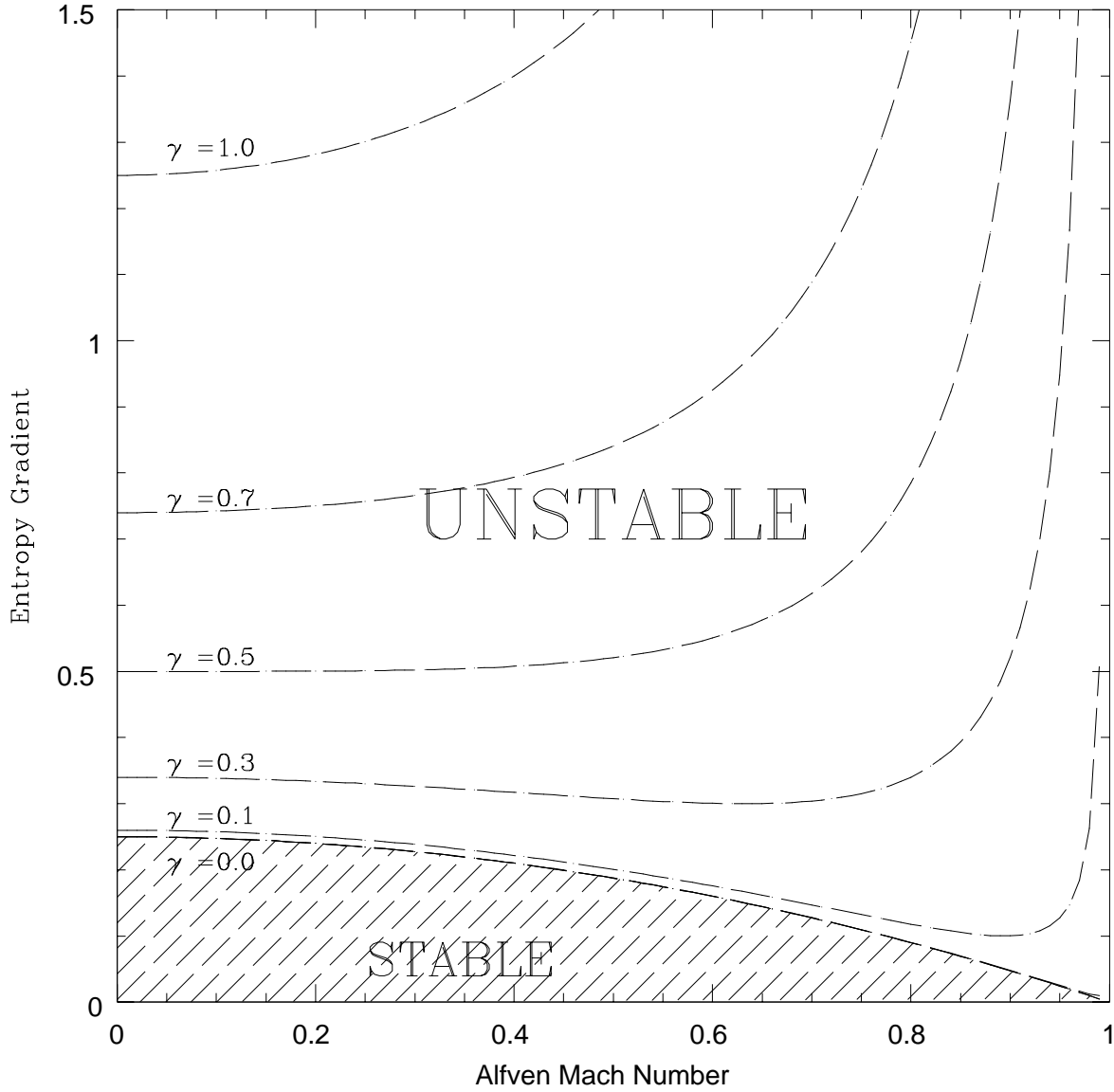


Fig. 3.— The stability diagram for the straight-field case as described by equation (51) in section 3.3. Note that the qualitative features of the diagram are similar to those in figure 2. A value of $L = \pi$ was chosen to plot this diagram.

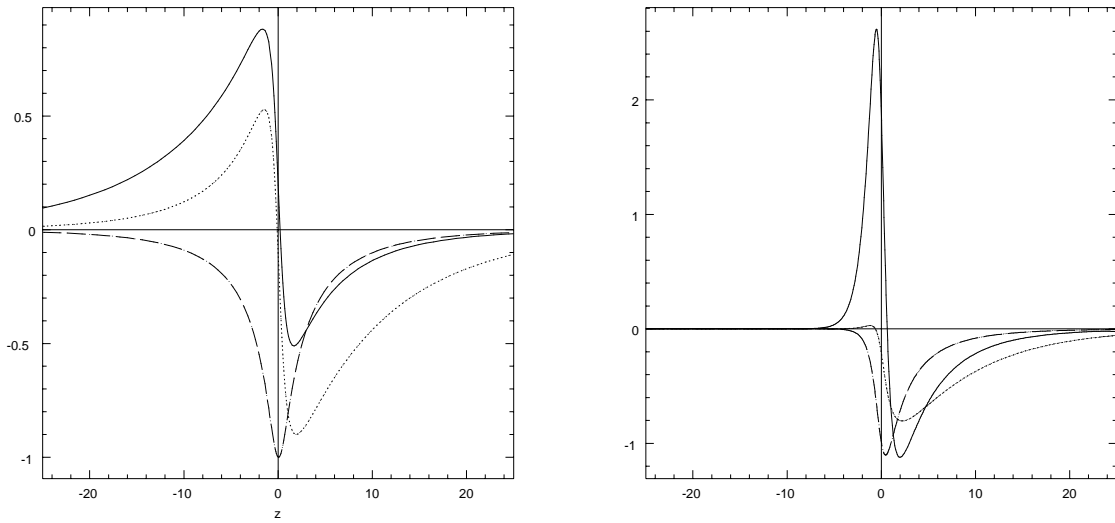


Fig. 4.— Eigenfunctions for entropy gradient $s'_0 = 0.6$ and $M = 0$ (left plot) and $M = 0.8$ (right plot). The three functions are A_+ (solid line), A_- (dotted line), and s (dashed line). Note that for the $M = 0.8$ case, where the plasma flow is in the $+z$ direction, the eigenfunctions grow quickly with steep gradients and diminish slowly as you move from left to right.

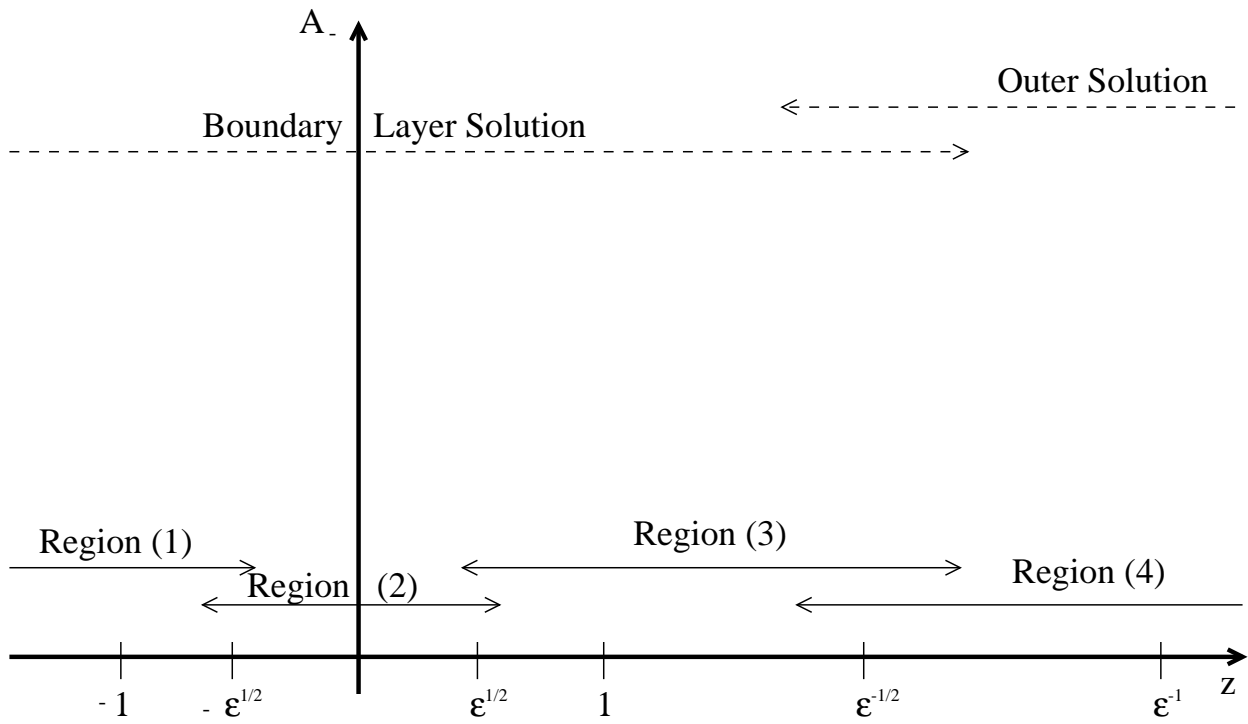


Fig. 5.— Regions defined for the asymptotic solution of A_- in the limit $M \rightarrow 1$.